Model for describing plasmonic nanolasers using Maxwell-Liouville equations with finite-difference time-domain calculations

Dhara J. Trivedi,[1] Danqing Wang,[2] Teri W. Odom,[1,2] and George C. Schatz[1,2,*]
[1]*Department of Chemistry, Northwestern University, Evanston, Illinois 60208, USA*
[2]*Graduate Program in Applied Physics, Northwestern University, Evanston, Illinois 60208, USA*
(Received 21 September 2017; published 10 November 2017)

We present a theoretical study of lasing action when plasmonic metallic structures that show lattice plasmon resonances are embedded in a gain medium. Our model combines classical electrodynamics for arrays of gold nanoparticles with a four-level quantum Liouville model of the laser dye photophysics. A numerical solution was implemented using finite-difference time-domain calculations coupled with a finite-difference solution to the Liouville equation. A particular focus of this work is the influence of dephasing in the quantum dynamics on the emission intensity at the threshold for lasing. We find that dephasing in the quantum system leads to reduced lasing emission, but with little effect on the long-term population inversion. Both electronic and vibrational dephasing is considered, but only electronic dephasing is significant, with the fully dephased result appearing for dephasing times comparable to plasmon dephasing ($\sim$10 fs) while fully coherent results involve $>$100 ps dephasing times as determined by the rate of stimulated emission. There are factor-of-2 differences between the Maxwell-Liouville results (greater emission intensities and narrower widths) compared to the corresponding results of rate-equation models of the dye states, which indicates the importance of using the Maxwell-Liouville approach in modeling these systems. We also examine rate-equation models with and without constraints arising from the Pauli exclusion principle, and we find relatively small effects.

DOI: 10.1103/PhysRevA.96.053825

I. INTRODUCTION

Studies of the optical properties of plasmonic nanostructures have gained a lot of attention due to their wide range of applications, including biochemical sensing [1,2], energy harvesting [3,4], light generation [5], near-field imaging [6,7], and nanoscale photochemistry [8,9]. The combination of surface-plasmon (SP) excitation of the plasmonic nanoparticles (NPs) with excitation of a molecular gain medium leads to additional optical functions, in particular, lasing action can occur in some situations [10–15]. While there are several possible platforms for plasmon laser research, one that has proven especially effective involves using narrow and sharp resonances known as lattice plasmons [16,17], in which the plasmonic particles are arranged in an array such that both diffraction and plasmon resonances can be excited simultaneously. Recent experimental studies have shown that stimulated emission by gain molecules in the presence of lattice plasmons is sufficiently enhanced that it overcomes losses from light absorption and other processes, yielding lasing action at relatively low intensities [10]. In addition to that, experimental research has shown lasing from a single plasmonic nanoparticle with a dye-doped core-shell structure [18] and a random [19], quasiperiodic, and aperiodic plasmonic lattice structure [20] in a dye-doped waveguide. However, lattice plasmon resonances have a higher-quality factor Q [21,22], and this makes it possible for periodic arrays coupled with a gain medium to show low-threshold room-temperature lasing, together with spatial coherence, directional emission normal to the surface, and tunability over near-infrared wavelengths [23,24].

A schematic diagram of a typical plasmonic nanocavity array laser is shown in Fig. 1. It is composed of a two-dimensional array of Au NPs patterned on a glass substrate and then covered by a polymer gain layer. This plasmon laser setup is similar to a cavity laser where the resonant cavity gets replaced by NPs. For both cavity and lattice plasmon lasers, it is desirable to have a theoretical model to describe the excited-state population dynamics and cavity electrodynamics so as to determine the optimum laser structure and choice of laser dye and excitation source for lasing. Many methods have now been proposed for this purpose [25–31], however, modeling the lattice plasmon lasers has continued to present important challenges and opportunities. The most common and successful approach has involved describing the electromagnetic fields using Maxwell's equations while treating the gain molecules with rate equations that govern the population dynamics. The populations are then assumed to drive the fields by assuming a phenomenological driven harmonic oscillator response for the polarization induced in the gain medium to the population inversion. To solve Maxwell's equations for the dynamics of the electromagnetic (EM) fields, the finite-difference time-domain (FDTD) method is the most used computational approach [32,33], and this can be connected nicely to a finite-difference solution to the rate equations and driven oscillator dynamics.

In addition to using rate equations for the atomic populations [25,33], Bloch equations have also been considered [31]. Although the Bloch equations lead to comprehensive studies of light-matter interactions, the number of levels involved constrains the computation [26,30,34]. So far the most complete theory for describing plasmonic lasing in nanocavity arrays was developed by Dridi *et al.* [28] by implementing the FDTD method in conjunction with a four-level description of the dye molecules, and the oscillator model coupling polarization to the local field. Despite its versatile and

*g-schatz@northwestern.edu

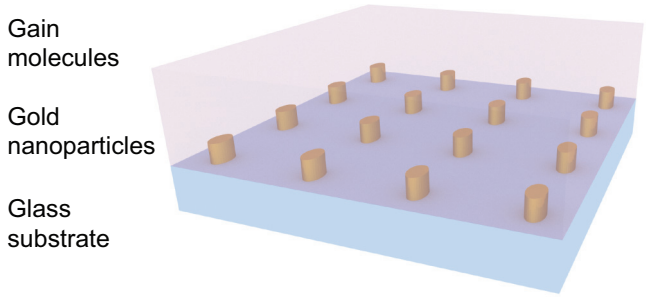

FIG. 1. Schematic representation of the nanoparticle array laser.

simple formulation, it cannot appropriately model dephasing in the quantum system, which is worrisome given that the time scale of dephasing is expected to be similar to that for plasmon dephasing in the classical electromagnetic field.

The interaction of light with a thermally fluctuating environment perturbs phase relationships in the quantum system, leading to dephasing of the quantum states, and ultimately decoherence of any coherent superpositions of quantum states [35,36] that is produced in the initial excitation of the system with an ultrafast laser. Dephasing is the central feature in the transition between quantum and classical behavior in any system [37,38]. Coherence loss is facilitated by a lack of phase-space structure [39], and becomes an irreversible phenomenon in systems with many degrees of freedom. Plasmon excitation is typically associated with rapid dephasing ($<$10 fs), and this dephasing effect is treated classically in the classical electrodynamics. However, the gain medium in the lattice plasmon laser can also dephase due to environmental interactions. Dephasing can affect lasing in two ways: It can destroy the lasing effect by decreasing the efficiency of energy exchange between plasmons and the gain medium, lowering population inversion. Also, it effectively broadens the molecular states that interact with the plasmons. If destructive effects dominate, lasing can either be quenched, or increased pumping is needed to achieve lasing. The effect of dephasing within such a system can be captured properly by considering the quantum dynamics of open systems, which extends the unitary evolution of the Schrödinger equation for the wave function into a nonunitary stochastic Schrödinger equation [40,41]. Alternatively, we can generalize to the quantum Liouville–von Neumann equation for the density matrix [42] in combination with solving Maxwell's equations for the field, the so-called Maxwell-Liouville method.

In this paper, we investigate the effect of gain molecule dephasing on the properties of lattice plasmon lasers. This is done using the Maxwell-Liouville approach, including the classical model of the polarization response to the applied field (which is based on the rotating-wave approximation). A detailed analysis of the effect of dephasing on populations and laser emission is presented, and we also make comparisons with the results of the established rate-equation methods. The paper is organized as follows: In Sec. II, we present the theoretical model describing lasing action based on the coupled Maxwell-Liouville equations. In Sec. III, we provide details of the numerical implementation. Section IV presents the study of an array of gold NPs embedded in a gain medium, including an analysis of the impact of various dephasing times on lasing. We also briefly compare our method with previously proposed methods for studying stimulated emission using classical rate equations, including methods that do or do not impose constraints associated with the Pauli exclusion principle. Finally, in Sec. V, we summarize our results with a future research outlook.

II. MODEL

We seek to understand the mechanism underlying the coupling and dynamics of EM fields of the nanoparticles and the quantized response of gain molecules in a lattice plasmon laser. The interaction of the EM field, induced due to the plasmonic system, with the gain medium can be split into two parts: the action of the EM wave on the molecule and the action of the molecule on the EM field. The gain medium consists of molecules that are initially in the ground state. The EM field of the incident ultrafast excitation pulse induces electronic transitions, and the excited-state photodynamics leads to transitions between energy levels that result in population inversion. In order to model all these effects in a self-consistent manner requires the simulation of coupled Maxwell-Liouville equations, providing a scheme for understanding the effects of dephasing on the evolution. The dynamics of the EM fields $\vec{E}$ and $\vec{H}$ is governed by Maxwell's equations,

$$\nabla \times \vec{E}(t) = -\mu_0 \frac{\partial \vec{H}(t)}{\partial t}, \tag{1}$$

$$\nabla \times \vec{H}(t) = \varepsilon \frac{\partial \vec{E}(t)}{\partial t} + \frac{\partial \vec{P}(t)}{\partial t}, \tag{2}$$

where μ_0 is the magnetic permeability of free space and ε is the dielectric permittivity. $\vec{P}$ is the net macroscopic polarization of the molecular system resulting from the EM field induced by optical transitions.

For a self-consistent interaction between the gain medium and the EM field, we need to determine the time evolution of the local molecular polarizability, which depends on the evolution of the molecular density matrix in the presence of the EM field. The net macroscopic polarization, induced due to population differences between pairs of optically coupled states, is locally driven by the electric field. In the rotating-wave approximation, the Heisenberg equation for the time evolution of the molecular polarization can be cast in the form of a classical electron oscillator model (see the Appendix), within the linear-response domain, leading to an equation for the time dependence of $\vec{P}$ given by [27,43]

$$\frac{d^2\vec{P}}{dt^2} + \Delta\omega \frac{d\vec{P}}{dt} + \omega^2 \vec{P} = \kappa N \Delta\rho(t) \vec{E}(t). \tag{3}$$

Here, $\Delta\omega$ is the bandwidth of the transition of interest, N is the number density of molecules in the gain medium, $\Delta\rho(t)$ is the fractional difference in the populations between the two energy levels that drive the polarization, $\kappa = 6\pi\epsilon_0 c^3/\omega^3\tau$, and τ is the lifetime of the spontaneous emission associated with the transition. Note that the right-hand side of Eq. (3) depends on population differences, i.e., diagonal elements of the density matrix, but not the off-diagonal density-matrix elements. This result, which comes by invoking the

rotating-wave approximation, plays a crucial role in determining the effect of dephasing in the quantum system on the evolution of the classical fields. While the rotating-wave approximation is not always satisfied, the primary deviations arise when the field-matter interactions are strong, which would not seem to be relevant to the threshold behavior of the laser systems we are considering.

As a next step, we need to determine the time evolution of the full density matrix. Assuming that the concentration of the quantum medium is low enough to neglect Coulomb interactions (leading to exciton transfer) between individual quantum systems, one can describe the quantum dynamics using the Liouville–von Neumann equation for a single molecule,

$$i\hbar\frac{d\hat{\rho}}{dt} = [\hat{H},\hat{\rho}] - i\hbar\hat{\Gamma}\hat{\rho}, \tag{4}$$

where $\hat{\rho}$ is the density matrix of the molecule and $\hat{H}$ is the total Hamiltonian, including the gain medium–EM field interaction term. The relaxation processes, described by the phenomenological operator $\hat{\Gamma}$, are considered to be Markovian [44]. The diagonal elements of it describe excited-state lifetimes, while nondiagonal elements account for dephasing effects. The Hamiltonian includes a time-independent free component $\hat{H}_0$ and a term describing the interaction with the electromagnetic field $\vec{E}(t)$,

$$\hat{H}(t) = \hat{H}_0 - \vec{d}\cdot\vec{E}(t), \tag{5}$$

where $\vec{d}$ is the dipole moment operator of the quantum system. This equation shows that the field-molecule interaction Hamiltonian depends on the angle between the electric field and transition dipole moment of the molecule. This angular dependence greatly impacts the threshold and intensity of the stimulated emission, but the trends are easy to understand so we assume that the two vectors are aligned in this work.

In order to fully describe the lasing dynamics we model each molecule as a four-level system with an optical transition for absorption (and emission) ($0 \leftrightarrow 3$) and for the emission (and absorption) ($2 \leftrightarrow 1$), based on the schematic energy diagram shown in Fig. 2. When the dye is optically pumped on the transition ($0 \leftrightarrow 3$), the four-level model will provide gain via stimulated emission for the transition ($2 \leftrightarrow 1$). The spontaneous decay rates of transitions between ($3 \rightarrow 2$) and ($1 \rightarrow 0$) are assumed to be fast enough that not enough population accumulates in states 3 and 1. On the other hand, the spontaneous decay rates for the transitions ($2 \rightarrow 1$) and ($3 \rightarrow 0$) are assumed to be small. Following a fast nonradiative transition ($3 \rightarrow 2$), population inversion is achieved. For sufficiently high incident field intensities [10,28], plasmon-driven stimulated emission associated with the $2 \leftrightarrow 1$ transition leads to lasing.

In order to understand this model it is convenient to think of the states 3 and 2 as vibrational states of the same excited electronic state, while states 1 and 0 are vibrational states of the ground electronic state. We will use the terms "electronic" and "vibrational" later in this paper in describing the results.

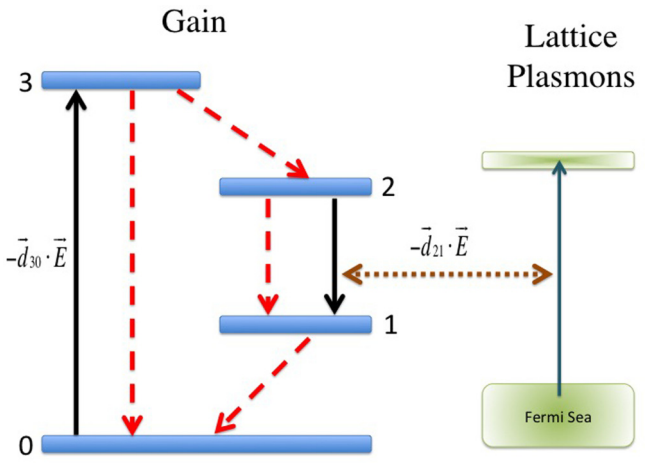

FIG. 2. Scheme showing the energy-transfer process for the optically excited four-level gain medium coupled to lattice plasmons in nanoparticle arrays: The dashed lines are for spontaneous transitions and continuous lines for stimulated transitions.

The Hamiltonian for the system can be written as

$$\hat{H} = \begin{pmatrix} \varepsilon_0 & 0 & 0 & \Omega_{03} \\ 0 & \varepsilon_1 & \Omega_{12} & 0 \\ 0 & \Omega_{21} & \varepsilon_2 & 0 \\ \Omega_{30} & 0 & 0 & \varepsilon_3 \end{pmatrix}, \tag{6}$$

where ε_i is the energy of ith energy level, and $\Omega = -\vec{d}_{ij}\cdot\vec{E}(t)$ is the coupling energy between two energy levels, with d_{ij} being the transition dipole moment between states i and j.

Equations (1)–(6) describe the self-consistent time evolution of interactions between the dye molecules and EM fields associated with the NP arrays. Equations (4) and (6) lead to coupled Maxwell-Liouville equations for the molecular density-matrix elements,

$$\frac{d\rho_{00}}{dt} = \frac{1}{i\hbar}(\Omega_{03}\rho_{30} - \Omega_{30}\rho_{03}) + \Delta_{30}\rho_{33} + \Delta_{10}\rho_{11}, \tag{7a}$$

$$\frac{d\rho_{01}}{dt} = \frac{1}{i\hbar}[\Omega_{03}\rho_{31} - \Omega_{21}\rho_{02} - \rho_{01}(\varepsilon_1 - \varepsilon_0)] - \gamma_{01}\rho_{01}, \tag{7b}$$

$$\frac{d\rho_{02}}{dt} = \frac{1}{i\hbar}[\Omega_{03}\rho_{32} - \Omega_{12}\rho_{01} - \rho_{02}(\varepsilon_2 - \varepsilon_0)] - \gamma_{02}\rho_{02}, \tag{7c}$$

$$\frac{d\rho_{03}}{dt} = \frac{1}{i\hbar}[\Omega_{03}(\rho_{33} - \rho_{00}) - \rho_{03}(\varepsilon_3 - \varepsilon_0)] - \gamma_{03}\rho_{03}, \tag{7d}$$

$$\frac{d\rho_{10}}{dt} = \frac{1}{i\hbar}[\Omega_{12}\rho_{20} - \Omega_{30}\rho_{13} + \rho_{10}(\varepsilon_1 - \varepsilon_0)] - \gamma_{10}\rho_{10}, \tag{7e}$$

$$\frac{d\rho_{11}}{dt} = \frac{1}{i\hbar}(\Omega_{12}\rho_{21} - \Omega_{21}\rho_{12}) - \Delta_{10}\rho_{11} + \Delta_{21}\rho_{22}, \tag{7f}$$

$$\frac{d\rho_{12}}{dt} = \frac{1}{i\hbar}[\Omega_{12}(\rho_{22} - \rho_{11}) - \rho_{12}(\varepsilon_2 - \varepsilon_1)] - \gamma_{12}\rho_{12}, \tag{7g}$$

$$\frac{d\rho_{13}}{dt} = \frac{1}{i\hbar}[\Omega_{12}\rho_{23} - \Omega_{03}\rho_{10} - \rho_{13}(\varepsilon_3 - \varepsilon_1)] - \gamma_{13}\rho_{13}, \tag{7h}$$

$$\frac{d\rho_{20}}{dt} = \frac{1}{i\hbar}[\Omega_{21}\rho_{10} - \Omega_{30}\rho_{23} + \rho_{20}(\varepsilon_2 - \varepsilon_0)] - \gamma_{20}\rho_{20}, \tag{7i}$$

$$\frac{d\rho_{21}}{dt} = \frac{1}{i\hbar}[\rho_{21}(\varepsilon_2 - \varepsilon_1) - \Omega_{21}(\rho_{22} - \rho_{11})] - \gamma_{21}\rho_{21}, \tag{7j}$$

$$\frac{d\rho_{22}}{dt} = \frac{1}{i\hbar}(\Omega_{21}\rho_{12} - \Omega_{12}\rho_{21}) - \Delta_{21}\rho_{22} + \Delta_{32}\rho_{33}, \tag{7k}$$

$$\frac{d\rho_{23}}{dt} = \frac{1}{i\hbar}[\Omega_{21}\rho_{13} - \Omega_{03}\rho_{20} - \rho_{23}(\varepsilon_3 - \varepsilon_2)] - \gamma_{23}\rho_{23}, \tag{7l}$$

$$\frac{d\rho_{30}}{dt} = \frac{1}{i\hbar}[\rho_{30}(\varepsilon_3 - \varepsilon_0) - \Omega_{30}(\rho_{33} - \rho_{00})] - \gamma_{30}\rho_{30}, \tag{7m}$$

$$\frac{d\rho_{31}}{dt} = \frac{1}{i\hbar}[\Omega_{30}\rho_{01} - \Omega_{21}\rho_{32} + \rho_{31}(\varepsilon_3 - \varepsilon_1)] - \gamma_{31}\rho_{31}, \tag{7n}$$

$$\frac{d\rho_{32}}{dt} = \frac{1}{i\hbar}[\Omega_{30}\rho_{02} - \Omega_{12}\rho_{31} + \rho_{32}(\varepsilon_3 - \varepsilon_2)] - \gamma_{32}\rho_{32}, \tag{7o}$$

$$\frac{d\rho_{33}}{dt} = \frac{1}{i\hbar}(\Omega_{30}\rho_{03} - \Omega_{03}\rho_{30}) - (\Delta_{30} + \Delta_{32})\rho_{33}, \tag{7p}$$

where Δ_{ij}'s are excited-state decay rates and γ_{ij}'s are dephasing rates between two energy levels, i and j.

Equations (7) show how the off-diagonal density-matrix elements get coupled to the populations through the Liouville equation. The electric field is coupled to these off-diagonal elements through the coupling in Eq. (5), so this provides the possibility for phases of the field to couple to coherences in the density matrix.

III. NUMERICAL DETAILS

To solve the above coupled Maxwell-Liouville equations, we employ an algorithm based on a finite-difference approach that generalizes the usual FDTD technique to include the time evolution of the density-matrix elements of the molecule. Initially proposed in Ref. [27], this approach has several attractive merits including simplicity, numerical stability, and applicability to objects with arbitrary geometry and optical properties.

The numerical implementation scheme to solve the coupled Maxwell-Liouville equations is as follows: (1) The magnetic field is determined via Faraday's law. Next, using the macroscopic polarization current density of the previous time step, the electric field is updated. (2) With knowledge of the local electric field components, we update the density matrix at each spatial point. (3) Finally, with knowledge of the electric field components and the updated density matrix, we calculate the macroscopic polarization current $\frac{d\vec{P}}{dt}$ at a corresponding grid point.

In the FDTD framework both electric and magnetic fields are propagated in time and space using the coupled Maxwell's curl equations based on the Yee algorithm [32,45]. Based on second-order central differences, the FDTD method implements the space derivatives of the curl operators via finite differences in regular interleaved three-dimensional Cartesian space meshes for the electromagnetic fields. $\vec{E}$ and $\vec{H}$ components are arranged in a leapfrog arrangement as a function of time in the three-dimensional (3D) grid. Hence, each $\vec{E}$ component is surrounded by four circulating $\vec{H}$ components and every $\vec{H}$ component is surrounded by four circulating $\vec{E}$ components. The molecular density-matrix and net macroscopic polarizations are calculated using the spatial average of the $\vec{E}$ components on adjacent half cells. In order to take into account the anisotropic simulation cells, the electric flux is computed to accurately determine the electric field [28,46].

The simulation cell has periodic boundary conditions in the x and y directions while a uniaxial perfect matched layer (UPML) [32] is used at the top and bottom to absorb waves at the cell boundaries.

To investigate the role of dephasing in our model, we consider the setup schematically shown in Fig. 1. This setup is identical to the one previously implemented in Ref. [28] using a rate-equation approach. The gold particles in this setup are cylinders with an elliptical cross section. The major axis, minor axis, and height of Au NPs are 100, 50, and 60 nm, respectively. The periodicity of the plasmonic structure along the x and y axis is 300 nm (square lattice), the refractive index of the surrounding medium is $n = 1.5$, and the thickness of the dye is 200 nm. A Drude-Lorentz fit function [47] is used to describe the complex dielectric function of gold.

The absorption (λ_{30}) and emission (λ_{21}) wavelengths of the dye are 600 and 720 nm, respectively. The spectral bandwidths of the emission and absorption transitions are both assumed to be 100 nm. The incident pulse is a Gaussian pulse centered at λ_{30} with a temporal bandwidth of 150 fs and is polarized along the major axis of the particles. The incident light is assumed to propagate along the z direction, which is normal to the NP array. The concentration of the dye is 2.5×10^{25} molecules m^{-3}, corresponding to 25 molecules in a 10-nm^3 cell. This is small enough that the energy transfer between molecules is too slow to play a role on the time scales of importance to this work. The emission spectrum is collected along the z direction (as dictated by the lattice plasmon diffraction condition) using a spatial average of the NP array in the time domain.

The spontaneous decay and dephasing rates depend on the energy difference between the levels under consideration. We empirically assign the time scales of spontaneous relaxation and dephasing in the present study. The spontaneous relaxation time scale between electronic states is assumed to be in the ns range (here we note that Purcell effects would shorten it, as considered previously [28], but the revised time scale would still be much longer than is important in this work), while it is taken to be in the fs range between vibrational states. The dephasing rates between two levels are expected to vary inversely with the energy spacing between them [48–50], so we have assumed the dephasing of vibrational states is in the ps range, while dephasing of the electronic states is in the fs range. The parameters we have chosen are listed in Table I. The

TABLE I. The spontaneous and dephasing relaxation time scales of various transitions.

Transitions	Spontaneous relaxation (Δ)	Transitions	Dephasing time scale (γ)
$3 \rightarrow 0$	1 ns	$3 \leftrightarrow 0$	2 fs
$3 \rightarrow 2$	10 fs	$3 \leftrightarrow 2$	0.2 ps
$2 \rightarrow 1$	1 ns	$2 \leftrightarrow 1$	2 fs
$1 \rightarrow 0$	10 fs	$1 \leftrightarrow 0$	0.2 ps

parameters for spontaneous decay are the same as implemented in Ref. [28]. Later in the paper we examine the sensitivity of the results to the choices of dephasing times.

IV. EFFECT OF DEPHASING ON LASING

In Fig. 3(a), we have plotted the extinction spectrum of the passive structure of Fig. 1. The broad peak near 730 nm is a typical lattice plasmon dipolar mode. The emission spectrum of the active medium, for the pump intensity above the threshold, is shown in Fig. 3(b). There are two distinct emission peaks in the spectrum: The first one is at $\lambda = 600$ nm, the absorption wavelength of the dye. It appears due to stimulated emission at the exciting wavelength as results from an incomplete loss of population in state 3 from the $3 \rightarrow 2$ transition. The second peak is at $\lambda = 732$ nm, corresponding to stimulated emission between states 2 and 1. The narrow emission profile along with the threshold behavior of the peak are typical of stimulated emission for the four-level model. In Fig. 3(c), we show the normalized state populations as a function of time after the initial pulse. Plasmon coupling with the gain medium leads to a steady population inversion

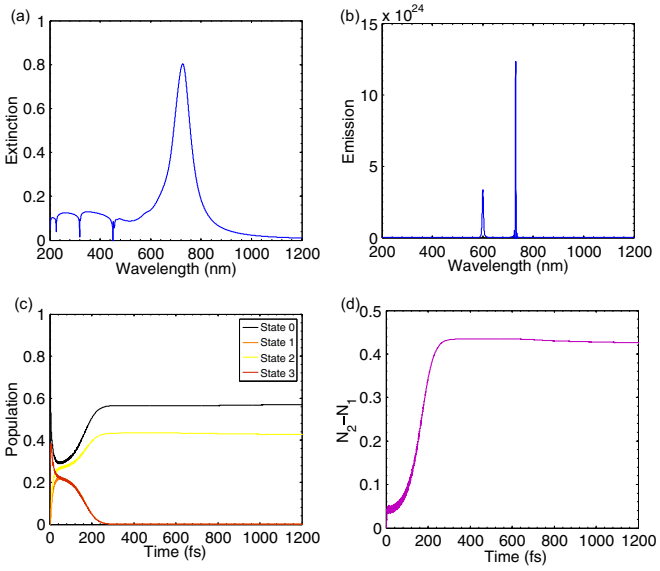

FIG. 3. (a) Extinction spectra of a passive structure. (b) Emission spectra of an active structure. (c) Time dependence of the occupation densities of the gain medium. (d) Time dependence of the normalized population inversion. The input pulse energy for these calculations is equal to 60 mJ cm^{-2}, corresponding to the threshold for lasing in this model.

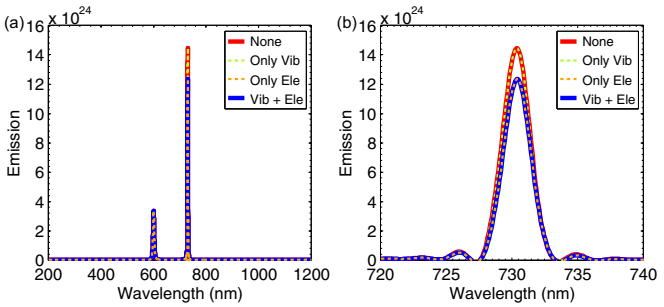

FIG. 4. Comparison between the impact of various types of dephasing on emission. Plots of (a) full emission profile and (b) zoomed version of stimulated emission peak. Red solid line, without any kind of dephasing; blue solid line, complete dephasing; green dotted line, only vibrational dephasing; orange dotted line, only electronic dephasing. Threshold for an input energy is equal to 60 mJ cm^{-2}.

that is essential for lasing. To be more precise, the term $\frac{1}{i\hbar}(\Omega_{21}\rho_{12} - \Omega_{12}\rho_{21})$ in Eq. 7(k) drives the inversion condition, essential for stimulated emission. This term modifies the population of the metastable state explicitly, which in turn modifies the local net polarization. In Fig. 3(d), we plot the population inversion between states 2 and 1, confirming the buildup of this inversion during the 150 fs of the initial pulse, and then its slow decay thereafter.

A. Electronic dephasing versus vibrational dephasing

Previous studies have demonstrated that dephasing affects the state populations [36,51] in the molecules and their coupling with the plasmonic field [52–54]. Since population inversion is a prerequisite for lasing, it is critical to understand the influence of dephasing on it. In addition, our model contains both electronic and vibrational dephasing, so it is important to study how each factor impacts the lasing dynamics.

Here, we study four cases in detail to investigate the influence of dephasing on steady-state population inversion and in turn on stimulated emission. In the first case, the system evolves coherently (no dephasing), and the results are labeled as None in Fig. 4. As a second case, we examine the dephasing only between vibrational levels, i.e., nonzero γ_{ij}'s in Eq. 7 using the value in Table I for levels 3 and 2 and 1 and 0, while the electronic levels stay in perfect coherence. As a third case, the vibrational levels stay in perfect coherence while decoherence between electronic states is taken into account, i.e., nonzero γ_{ij}'s for levels 2 and 1 and 3 and 0. In the fourth scenario, all levels lose coherence simultaneously with the values in Table I. In Fig. 4(a), we plot the emission spectra in all four cases. It is evident from the figure that electronic dephasing influences the intensity of stimulated emission [Fig. 4(b)], but dephasing between vibrational states has no affect. This outcome is understandable, as the assumed time scale for vibrational dephasing is much longer than the time scale for spontaneous relaxation for the 3 and 2 and 1 and 0 transitions, so vibrational dephasing should have no effect. Meanwhile the time scale for electronic dephasing is much shorter than the relaxation time, so this has a bigger effect

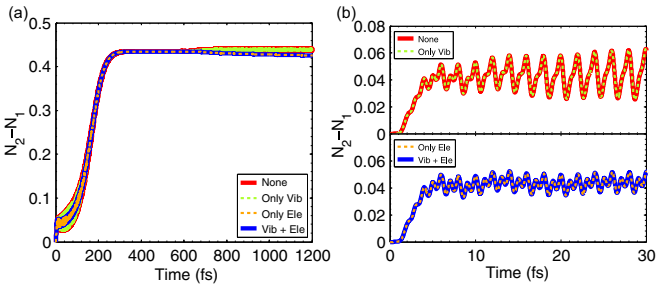

FIG. 5. Comparison between the impact of various types of dephasing on steady-state population inversion as a function of time. (b) Plot of the first 30 fs of the dynamics. Red solid line, without any kind of dephasing; blue solid line, complete dephasing; green dotted line, only vibrational dephasing; orange dotted line, only electronic dephasing. The input pulse energy is 60 mJ cm^{-2}, which is just above the laser threshold.

(though only reducing the intensity by only about 10%). Also note that the peak near 600 nm is robust under dephasing, as this peak is a result of pump-driven transitions and is very short lived.

In Fig. 5(a), we have plotted the normalized steady-state population inversion for the four choices of dephasing times. This shows that the population oscillates rapidly, between levels 2 and 1, for the first ∼150 fs, corresponding to the time when the pump is on. From Fig. 5(b) it is evident that electronic dephasing dampens the oscillations in the population inversion during the first 30 fs, while vibrational dephasing has no effect (matching the fully coherent results during this time interval). At times longer than about 200 fs, the populations are all very similar, which suggests that the initial differences at short times do not significantly affect the longer time-scale population inversion.

We further systematically study the impact of vibrational and electronic dephasing to investigate convergence behavior. In the first scenario, we decrease the coherence time between vibrational levels to explore the impact of vibrational dephasing, fixing the electronic dephasing time at 2 fs. The results are plotted in Fig. 6(a). It is evident from the spectra that vibrational dephasing even at the time scale of 2 as does not influence stimulated emission.

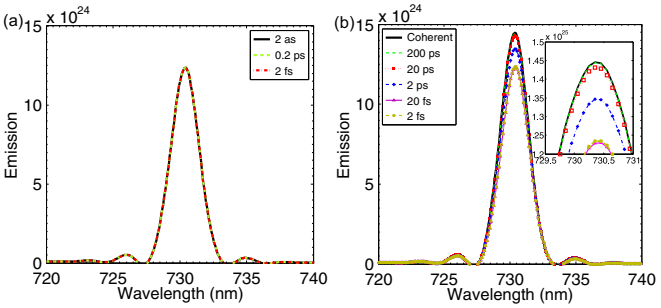

FIG. 6. Plot of stimulated emission peak (a) for different vibrational dephasing time scales, with constant 2 fs electronic dephasing, and (b) for different electronic dephasing time scales, with constant 200-fs vibrational dephasing. In the inset, the curves are ordered from top to bottom, going from 200 ps (top) to 2 fs (bottom).

To explore the convergence behavior for electronic dephasing, we keep the vibrational dephasing time at 200 fs and gradually increase the electronic dephasing time. The emission spectra in this case are plotted in Fig. 6(b). It is evident from the results (see the inset to the figure) that, unlike vibrational dephasing, the time scale of electronic dephasing strongly influences the peak stimulated emission intensity, with fully dephased results being obtained for dephasing times on the order of 10 fs, and fully coherent results obtained for dephasing times greater than 100 ps. In between these two limits there is a smooth transition in peak emission from dephased to coherent limits. Note that the 100-ps coherent time scale is faster than the $2 \rightarrow 1$ radiative lifetime, reflecting the fact that at the lasing threshold stimulated emission is faster than spontaneous emission. At the same time, the 10-fs limit for fully dephased results is comparable to the plasmon dephasing time.

B. Classical rate equation and density-matrix rate equation

In this section, we compare our method with previously established rate-equation approaches developed by Chang *et al.* [25] and Dridi *et al.* [28]. Chang's model is based on a four-level system in which there are two interacting electrons of the same spin. As a result, transitions between energy levels are governed by coupled rate equations that include a factor of $(1 - N)$ in the spontaneous emission rates to describe the effect of the Pauli exclusion principle (PEP) on allowed transitions. The time dependence of the populations is given by

$$\frac{dN_3}{dt} = -\frac{N_3(1-N_2)}{\tau_{32}} - \frac{N_3(1-N_0)}{\tau_{30}} + \frac{1}{\hbar\omega_{30}}\vec{E}\cdot\frac{d\vec{P}_{30}}{dt}, \tag{8a}$$

$$\frac{dN_2}{dt} = \frac{N_3(1-N_2)}{\tau_{32}} - \frac{N_2(1-N_1)}{\tau_{21}} + \frac{1}{\hbar\omega_{21}}\vec{E}\cdot\frac{d\vec{P}_{21}}{dt}, \tag{8b}$$

$$\frac{dN_1}{dt} = \frac{N_2(1-N_1)}{\tau_{21}} - \frac{N_1(1-N_0)}{\tau_{10}} - \frac{1}{\hbar\omega_{21}}\vec{E}\cdot\frac{d\vec{P}_{21}}{dt}, \tag{8c}$$

$$\frac{dN_0}{dt} = \frac{N_3(1-N_0)}{\tau_{30}} + \frac{N_1(1-N_0)}{\tau_{10}} - \frac{1}{\hbar\omega_{30}}\vec{E}\cdot\frac{d\vec{P}_{30}}{dt}. \tag{8d}$$

The PEP model has been widely used in describing semiconductor lasers, but its applicability to dye molecules is unknown.

The method developed by Dridi and Schatz is based on combining EM fields with a four-level description governed by a one-electron system in which the Pauli principle plays no role. The time evolution of electron population is determined using the rate equations

$$\frac{dN_3}{dt} = -\frac{N_3(t)}{\tau_{32}} - \frac{N_3(t)}{\tau_{30}} + \frac{1}{\hbar\omega_{30}}\vec{E}\cdot\frac{d\vec{P}_{30}}{dt}, \tag{9a}$$

$$\frac{dN_2}{dt} = \frac{N_3(t)}{\tau_{32}} - \frac{N_2(t)}{\tau_{21}} + \frac{1}{\hbar\omega_{21}}\vec{E}\cdot\frac{d\vec{P}_{21}}{dt}, \tag{9b}$$

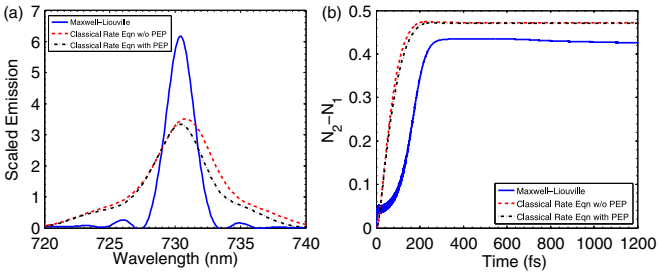

FIG. 7. (a) Stimulated emission peak and (b) steady-state condition of population inversion. The emission profile is normalized to the same input energy.

$$\frac{dN_1}{dt} = \frac{N_2(t)}{\tau_{21}} - \frac{N_1(t)}{\tau_{10}} - \frac{1}{\hbar\omega_{21}}\vec{E}\cdot\frac{d\vec{P}_{21}}{dt}, \tag{9c}$$

$$\frac{dN_0}{dt} = \frac{N_3(t)}{\tau_{30}} + \frac{N_1(t)}{\tau_{10}} - \frac{1}{\hbar\omega_{30}}\vec{E}\cdot\frac{d\vec{P}_{30}}{dt}. \tag{9d}$$

Note that the spontaneous rates in these equations are equivalent to our density-matrix model in the limit of a fully decohered system at all times. However, we note that even in this limit, the Liouville and rate-equation models are not precisely the same, as there is a Markovian approximation in addition to fast dephasing in converting the Liouville equation formalism to rate equations.

Figure 7 presents the direct comparison of these models with our method. Both types of dephasing, electronic and vibrational, have been included while solving the Maxwell-Liouville equations, using the parameters presented earlier (Table I). Note that the threshold powers needed in the three cases are slightly different, so results are normalized to the same incident pump energy. What we see from the figures are stimulated emission profiles obtained from the two rate-equation methods that are comparable [Fig. 7(a)], however, both sets of rate-equation results have a peak emission rate that is about half that of the Liouville equation result. In addition, the Liouville equation result is narrower. The steady-state population inversion condition [Fig. 7(b)] in all three cases is achieved around the same time scale, as makes sense given that the 150-fs pump plays a major role in producing this result, but it is in contrast to the results of previous attempts to include dephasing in lasing models [26].

The good agreement of the PEP and non-PEP rate-equation results arises because the state populations are generally low, which means that the influence of the $1 - N$ term in the PEP model is insignificant. In the Maxwell-Liouville method, the presence of initially oscillating behavior is a signature of initial coherent excitation [26]. At times above 200 fs, the Maxwell-Liouville population inversion is smaller than the rate-equation result, which means that the rate-equation results will tend to underestimate the lasing threshold.

V. CONCLUSIONS

In this paper, we have presented an approach to model plasmon-enhanced laser systems using a self-consistent electrodynamical model based on coupled Maxwell-Liouville equations. This model goes beyond earlier models of lattice plasmon lasers through its incorporation of dephasing effects in the quantum system (the gain medium), which allows us to study the transition from coherent to decohered evolution of the system during and after ultrafast excitation and lasing. The proposed model is applied to investigate a four-level density-matrix description of an active medium which allows for both electronic and vibrational excitation of the laser dye molecules.

We have applied our model to study arrays of gold NPs embedded in a gain medium to investigate the emission spectra of the active structure under circumstances where lattice plasmon resonance excitation leads to strongly enhanced stimulated emission. We present a detailed study of the correlation between dephasing rates and stimulated emission, showing that rapid dephasing between various energy levels changes the population inversion behavior at short times as well as reducing the amplitude of the lasing peak. We find that fast dephasing (on the order of 10 fs or less) between levels 2 and 1 (the states associated with the population inversion) has the most impact on reducing the intensity of stimulated emission, with emission intensities that are 10% smaller than for the fully coherent limit that arises for electronic dephasing times above 100 ps. The lasing behavior is even less sensitive to vibrational dephasing effects.

One possible reason for small dephasing effects is that in the rotating-wave approximation leading to Eq. (3), there is no phase dependence in the coupling between the plasmonic field and the induced polarization in the quantum system. Since the rotating-wave approximation is likely to be valid for the low-intensity lasers that have been studied so far, this result supports the earlier studies based on rate-equation models. However, the comparison of Maxwell-Liouville and rate equation results was less quantitative (factor-of-2 differences), which indicates that differences between the theories are driven by effects beyond vibrational or electronic dephasing, such as the Markovian approximation. Also, we found that rate-equation models that include the Pauli exclusion principle lead to results with only small differences compared to those that do not, due to the low occupation numbers associated with the dye laser structures we studied.

Our method provides a detailed description of lasing action in coupled plasmonic NP arrays, and other plasmonic systems with gain molecules. In addition, the method is versatile and easily extended to study interactions between other gain media (semiconductors) and plasmons. The code we have developed can consider random, quasiperiodic, and aperiodic structures for the plasmonic nanoparticles with little modification of the code. The technique should therefore be of general use for interpreting, predicting, and controlling the interactions in novel nanoscale nanoplasmonic lasers and other optical devices.

ACKNOWLEDGMENTS

These Liouville equation studies were supported by the U. S. Department of Energy, Basic Energy Sciences, under Grant No. DE-SC0004752 (D.J.T., G.C.S.). The classical rate-equation work was supported by National Science Foundation (DMR-1608258; D.W., T.W.O.). The authors thank M. Dridi for valuable comments.

APPENDIX: DERIVATION OF NET MACROSCOPIC MOLECULAR POLARIZATION

Here, we present a detailed derivation of the net macroscopic molecular polarizations associated with the emission and absorption transitions. The optically pumped transition leads to a microscopic polarization of the molecule that can be described by a classical electron oscillator (CEO) model using the equation of motion. Within the linear frequency domain, it has been generalized to account for a population of molecules that under an EM field oscillate at the same resonance frequency as the individual molecules. Although these equations has been previously derived in Refs. [25,27], here we are attaching a detailed derivation with the purpose of simplicity and consistency of the paper.

The atom-photon Hamiltonian for a two-level system can be expressed as

$$\hat{H} = \hat{H}_{\text{Atom}} + \hat{H}_{\text{Field}} + \hat{H}_{\text{AF}}, \tag{A1}$$

where $\hat{H}_{\text{Atom}} = \hbar\omega_a \hat{N}_u$, $\hat{H}_{\text{Field}} = \Sigma_k \hbar\omega_k(\hat{a}_k^\dagger \hat{a}_k + \frac{1}{2})$, and $\hat{H}_{\text{AF}} = -\hat{\mu}\cdot\hat{E}$. $\hat{N}_u = |u\rangle\langle u|$ is the number operator for the upper level $|u\rangle$. $\hat{N}_g = |g\rangle\langle g|$ is the number operator for the ground level $|g\rangle$. $\hbar\omega_a$ is the energy difference between $|u\rangle$ and $|g\rangle$. $\hat{a}_k^\dagger$ is the photon creation operator.

The electric field is given by,

$$\hat{E} = -\frac{d\hat{A}}{dt} = i\sum_k \sqrt{\frac{\hbar\omega_k}{2\varepsilon_0 v}}\mathbf{e}_k(\hat{a}_k e^{i\vec{k}\cdot\vec{x}} - \hat{a}_k^\dagger e^{-i\vec{k}\cdot\vec{x}}), \tag{A2}$$

with $\omega_k = \frac{|k|\cdot c}{n}$, and n is the refractive index of the medium.

The dipole operator is

$$\hat{\mu} = -e\hat{\mathbf{r}} = \sum_{\ell\ell'} \mu_{\ell\ell'}\hat{V}_{\ell\ell'}, \tag{A3}$$

where e is the electron charge and $\hat{V}_{\ell\ell'} = |\ell\rangle\langle\ell'|$ is the atomic transition operator. For a two-level system the dipole operator reduces to

$$\hat{\mu} = \mu\hat{V}^\dagger + \mu^*\hat{V}, \tag{A4}$$

with $\mu = \langle u|e\hat{r}|g\rangle = d\hat{\mathbf{e}}_z$ and $\hat{V} = |g\rangle\langle u|$.

From the second quantized Hamiltonian, we will derive the Heisenberg equation for motion for the atomic transition operator,

$$\frac{d\hat{V}}{dt} = \frac{i}{\hbar}[\hat{H}, \hat{V}]. \tag{A5}$$

Let us solve it for a two-level system term by term,

$$\begin{aligned}\frac{i}{\hbar}[\hat{H}_{\text{Atom}}, \hat{V}] &= \frac{i}{\hbar}(\hat{H}_{\text{Atom}}\hat{V} - \hat{V}\hat{H}_{\text{Atom}}) \\ &= \left(\frac{i}{\hbar}\right)(\hbar\omega_a)(\hat{N}_u|g\rangle\langle u| - |g\rangle\langle u|\hat{N}_u) \\ &= -i\omega_a\hat{V},\end{aligned} \tag{A6}$$

using $\langle\alpha|\beta\rangle = \delta_{\alpha,\beta}$.

The next term,

$$\begin{aligned}\frac{i}{\hbar}[\hat{H}_{\text{Field}}, \hat{V}] = \frac{i}{\hbar}\Bigg[&\sum_k \hbar\omega_k\left(\hat{a}_k^\dagger\hat{a}_k + \frac{1}{2}\right)|g\rangle\langle u| \\ &- |g\rangle\langle u|\sum_k \hbar\omega_k\left(\hat{a}_k^\dagger\hat{a}_k + \frac{1}{2}\right)\Bigg] \\ &= 0,\end{aligned} \tag{A7}$$

using $\hat{a}|g\rangle = 0$ and $\hat{a}^\dagger|u\rangle = 0$.

For the atom-field interaction term,

$$\begin{aligned}\frac{i}{\hbar}[\hat{H}_{\text{AF}}, \hat{V}] &= -\frac{i}{\hbar}[\hat{\mu}\cdot\hat{E}, \hat{V}] \\ &= -\frac{i}{\hbar}[(\mu\hat{V}^\dagger + \mu^*\hat{V})\cdot\hat{E}, \hat{V}] \\ &= -\frac{i}{\hbar}[(\mu\hat{V}^\dagger + \mu^*\hat{V}), \hat{V}]\cdot\hat{E} \\ &= -\frac{i}{\hbar}[(\mu\hat{V}^\dagger + \mu^*\hat{V})\hat{V} - \hat{V}(\mu\hat{V}^\dagger + \mu^*\hat{V})]\cdot\hat{E} \\ &= -\frac{i}{\hbar}\mu(\hat{V}^\dagger\hat{V} - \hat{V}\hat{V}^\dagger)\cdot\hat{E}.\end{aligned} \tag{A8}$$

Next,

$$\hat{V}^\dagger\hat{V} = |u\rangle\langle g||g\rangle\langle u| = \hat{N}_u, \tag{A9}$$

$$\hat{V}\hat{V}^\dagger = \hat{N}_g, \tag{A10}$$

$$\hat{V}^\dagger\hat{V}^\dagger = \hat{V}\hat{V} = 0. \tag{A11}$$

Using Eqs. (A9)–(A11) in Eq. (A8),

$$\frac{i}{\hbar}[\hat{H}_{\text{AF}}, \hat{V}] = -\frac{i}{\hbar}[\hat{\mu}\cdot\hat{E}, \hat{V}] = -\frac{i}{\hbar}\mu(\hat{N}_u - \hat{N}_g)\cdot\hat{\mathbf{E}}. \tag{A12}$$

Substituting Eqs. (A6), (A7), and (A12) in Eq. (A5),

$$\frac{d\hat{V}}{dt} = -i\omega_a\hat{V} - \frac{i}{\hbar}\hbar\mu(\hat{N}_u - \hat{N}_g)\cdot\hat{\mathbf{E}} - \gamma\hat{V}. \tag{A13}$$

The last term is the damping term and is empirically added in Eq. (A13). Similarly,

$$\frac{d\hat{V}^\dagger}{dt} = i\omega_a\hat{V}^\dagger - \frac{i}{\hbar}\mu^*(\hat{N}_u - \hat{N}_g)\cdot\hat{\mathbf{E}} - \gamma\hat{V}^\dagger. \tag{A14}$$

From Eq. (A4),

$$\begin{aligned}\frac{d\hat{\mu}}{dt} &= \mu\frac{d\hat{V}^\dagger}{dt} + \mu^*\frac{d\hat{V}}{dt} \\ &= \mu\left[i\omega_a\hat{V}^\dagger - \frac{i}{\hbar}\mu^*(\hat{N}_u - \hat{N}_g)\cdot\hat{\mathbf{E}} - \gamma\hat{V}^\dagger\right] \\ &\quad + \mu^*\left[-i\omega_a\hat{V} - \frac{i}{\hbar}\mu(\hat{N}_u - \hat{N}_g)\cdot\hat{\mathbf{E}} - \gamma\hat{V}\right] \\ &= i\omega_a(\mu\hat{V}^\dagger - \mu^*\hat{V}) - \gamma\hat{\mu} - \frac{2i}{\hbar}|d|^2(\hat{N}_u - \hat{N}_g)(\mathbf{e}_z\cdot\hat{\mathbf{E}}).\end{aligned} \tag{A15}$$

Next, taking the time derivative of Eq. (A15),

$$\frac{d^2\hat{\mu}}{dt^2} = i\omega_a \frac{d(\mu\hat{V}^\dagger - \mu^*\hat{V})}{dt} - \gamma\frac{d\hat{\mu}}{dt} - \frac{2i}{\hbar}|d|^2(\hat{N}_u - \hat{N}_g)\left(\mathbf{e}_z \cdot \frac{d\hat{\mathbf{E}}}{dt}\right) - \frac{2i}{\hbar}|d|^2\left(\frac{d\hat{N}_u}{dt} - \frac{d\hat{N}_g}{dt}\right)(\mathbf{e}_z \cdot \hat{\mathbf{E}}). \quad \text{(A16)}$$

Now,

$$\frac{d(\mu\hat{V}^\dagger - \mu^*\hat{V})}{dt} = \mu\frac{d\hat{V}^\dagger}{dt} - \mu^*\frac{d\hat{V}}{dt} = i\omega_a(\mu\hat{V}^\dagger + \mu^*\hat{V}) = i\omega_a\hat{\mu}. \quad \text{(A17)}$$

The population transition rate equations between levels can be achieved from the Heisenberg equation for motion,

$$\frac{d\hat{N}_u}{dt} = -\frac{d\hat{N}_g}{dt} = -\frac{i}{\hbar}\hat{\mu}\cdot\hat{E}. \quad \text{(A18)}$$

Substituting Eqs. (A17) and (A18) in Eq. (A16),

$$\frac{d^2\hat{\mu}}{dt^2} = -\omega_a^2\hat{\mu} - \gamma\frac{d\hat{\mu}}{dt} - \frac{2i}{\hbar}|d|^2(\hat{N}_u - \hat{N}_g)\left(\mathbf{e}_z \cdot \frac{d\hat{\mathbf{E}}}{dt}\right) - \frac{2i}{\hbar}|d|^2\left(-\frac{2i}{\hbar}\hat{\mu}\cdot\hat{E}\right)(\mathbf{e}_z \cdot \hat{\mathbf{E}}). \quad \text{(A19)}$$

Hence one recovers

$$\frac{d^2\hat{\mu}}{dt^2} + 2\gamma\frac{d\hat{\mu}}{dt} + \left[\omega_a^2 + \left(\frac{2|d|}{\hbar}\right)^2\hat{E}^2\right]\hat{\mu} = \frac{2i}{\hbar}|d|^2(\hat{N}_g - \hat{N}_u)\left(\mathbf{e}_z \cdot \frac{d\hat{\mathbf{E}}}{dt}\right). \quad \text{(A20)}$$

The additional γ term is added empirically in the equation.

[1] J. N. Anker, W. P. Hall, O. Lyandres, N. C. Shah, J. Zhao, and R. P. van Duyne, Nat. Mater. **7**, 442 (2008).
[2] S. A. Maier, *Plasmonics: Fundamentals and Applications* (Springer, Berlin, 2007).
[3] K. Catchpole and A. Polman, Opt. Express **16**, 21793 (2008).
[4] S. Mokkapati, F. Beck, R. de Waele, A. Polman, and K. Catchpole, J. Phys. D **44**, 185101 (2011).
[5] K. Okamoto, I. Niki, A. Shvartser, Y. Narukawa, T. Mukai, and A. Scherer, Nat. Mater. **3**, 601 (2004).
[6] A. V. Zayats and I. I. Smolyaninov, J. Opt. A **5**, S16 (2003).
[7] M. R. Beversluis, A. Bouhelier, and L. Novotny, Phys. Rev. B **68**, 115433 (2003).
[8] P. Christopher, H. Xin, and S. Linic, Nat. Chem. **3**, 467 (2011).
[9] H. Chen, M. A. Ratner, and G. C. Schatz, J. Photochem. Photobiol., A **221**, 143 (2011).
[10] W. Zhou, M. Dridi, J. Y. Suh, C. H. Kim, D. T. Co, M. R. Wasielewski, G. C. Schatz, T. W. Odom *et al.*, Nat. Nanotechnol. **8**, 506 (2013).
[11] P. Berini and I. de Leon, Nat. Photonics **6**, 16 (2011).
[12] J. Seidel, S. Grafström, and L. Eng, Phys. Rev. Lett. **94**, 177401 (2005).
[13] M. A. Noginov, G. Zhu, M. Mayy, B. A. Ritzo, N. Noginova, and V. A. Podolskiy, Phys. Rev. Lett. **101**, 226806 (2008).
[14] R. F. Oulton, V. J. Sorger, T. Zentgraf, R.-M. Ma, C. Gladden, L. Dai, G. Bartal, and X. Zhang, Nature (London) **461**, 629 (2009).
[15] A. Yang, Z. Li, M. P. Knudson, A. J. Hryn, W. Wang, K. Aydin, and T. W. Odom, ACS Nano **9**, 11582 (2015).
[16] M. Hentschel, M. Saliba, R. Vogelgesang, H. Giessen, A. P. Alivisatos, and N. Liu, Nano Lett. **10**, 2721 (2010).
[17] M. Hentschel, D. Dregely, R. Vogelgesang, H. Giessen, and N. Liu, ACS Nano **5**, 2042 (2011).
[18] M. A. Noginov, G. Zhu, A. M. Belgrave, R. Bakker, V. M. Shalaev, E. E. Narimanov, S. Stout, E. Herz, T. Suteewong, and U. Wiesner, Nature (London) **460**, 1110 (2009).
[19] A. H. Schokker and A. F. Koenderink, ACS Photonics **2**, 1289 (2015).
[20] A. H. Schokker and A. F. Koenderink, Optica **3**, 686 (2016).
[21] B. Auguié and W. L. Barnes, Phys. Rev. Lett. **101**, 143902 (2008).
[22] V. G. Kravets, F. Schedin, and A. N. Grigorenko, Phys. Rev. Lett. **101**, 087403 (2008).
[23] A. Yang, T. B. Hoang, M. Dridi, C. Deeb, M. H. Mikkelsen, G. C. Schatz, and T. W. Odom, Nat. Commun. **6**, 6939 (2015).
[24] P. Törmä, Nat. Nanotechnol. **12**, 838 (2017).
[25] S.-H. Chang and A. Taflove, Opt. Express **12**, 3827 (2004).
[26] G. M. Slavcheva, J. M. Arnold, and R. W. Ziolkowski, IEEE J. Sel. Top. Quantum Electron. **10**, 1052 (2004).
[27] Y. Huang and S.-T. Ho, Opt. Express **14**, 3569 (2006).
[28] M. Dridi and G. C. Schatz, J. Opt. Soc. Am. B **30**, 2791 (2013).
[29] A. Pusch, S. Wuestner, J. M. Hamm, K. L. Tsakmakidis, and O. Hess, ACS Nano **6**, 2420 (2012).
[30] S. Wuestner, A. Pusch, K. L. Tsakmakidis, J. M. Hamm, and O. Hess, Philos. Trans. R. Soc., A **369**, 3525 (2011).
[31] R. W. Ziolkowski, J. M. Arnold, and D. M. Gogny, Phys. Rev. A **52**, 3082 (1995).
[32] A. Taflove and S. C. Hagness, *Computational Electrodynamics* (Artech House, Boston, 2005).
[33] A. S. Nagra and R. A. York, IEEE Trans. Antennas Propag. **46**, 334 (1998).
[34] A. Fratalocchi, C. Conti, and G. Ruocco, Phys. Rev. A **78**, 013806 (2008).
[35] A. J. Leggett, S. Chakravarty, A. Dorsey, M. P. Fisher, A. Garg, and W. Zwerger, Rev. Mod. Phys. **59**, 1 (1987).
[36] W. H. Zurek, Rev. Mod. Phys. **75**, 715 (2003).
[37] J. Maddox, Nature (London) **373**, 469 (1995).
[38] J. Caro and L. L. Salcedo, Phys. Rev. A **60**, 842 (1999).
[39] A. K. Pattanayak and P. Brumer, Phys. Rev. Lett. **79**, 4131 (1997).
[40] E. Lorin, S. Chelkowski, and A. Bandrauk, Comput. Phys. Commun. **177**, 908 (2007).
[41] K. Lopata and D. Neuhauser, J. Chem. Phys. **130**, 104707 (2009).

[42] S. Chang and V. Minogin, Phys. Rep. **365**, 65 (2002).
[43] A. E. Siegman, *Lasers* (University Science, Mill Valley, CA, 1986).
[44] H.-P. Breuer and F. Petruccione, *The Theory of Open Quantum Systems* (Oxford University Press, Oxford, UK, 2002).
[45] K. Yee, IEEE Trans. Antennas Propag. **14**, 302 (1966).
[46] M. Dridi and G. C. Schatz, J. Opt. Soc. Am. B **32**, 818 (2015).
[47] A. Vial, A.-S. Grimault, D. Macías, D. Barchiesi, and M. L. de la Chapelle, Phys. Rev. B **71**, 085416 (2005).
[48] L. A. Pachón and P. Brumer, J. Phys. Chem. Lett. **2**, 2728 (2011).
[49] I. Franco, A. Rubio, and P. Brumer, New J. Phys. **15**, 043004 (2013).
[50] A. Kar, L. Chen, and I. Franco, J. Phys. Chem. Lett. **7**, 1616 (2016).
[51] G. S. Agarwal, M. O. Scully, and H. Walther, Phys. Rev. Lett. **86**, 4271 (2001).
[52] J. A. Hutchison, T. Schwartz, C. Genet, E. Devaux, and T. W. Ebbesen, Angew. Chem., Int. Ed. **51**, 1592 (2012).
[53] J. P. Long and B. Simpkins, ACS Photonics **2**, 130 (2014).
[54] A. Shalabney, J. George, J. Hutchison, G. Pupillo, C. Genet, and T. W. Ebbesen, Nat. Commun. **6**, 5981 (2015).